



A comparative analysis of Cr(VI) reduction with Cu_2O , ZnO and Fe_2O_3 coatings grown by PEO

Análisis comparativo de la reducción de Cr(VI) con Cu_2O , ZnO y Fe_2O_3 crecidos por OEP

Fernando Gordillo-Delgado ^{1, 2*} John Alexander García-Giraldo ¹

¹Grupo de Investigación en Ciencia Aplicada para el Desarrollo de la Ecorregión (GICADE), Instituto Interdisciplinario de las Ciencias, Universidad del Quindío. Carrera 15 # 12N. C. P 630004. Quindío, Colombia.

²Programa de Tecnología en Instrumentación Electrónica de la Facultad de Ciencias Básicas y Tecnologías, Universidad del Quindío. Carrera 15 # 12N. C. P 630004. Quindío, Colombia.

CITE THIS ARTICLE AS:

F. Gordillo-Delgado and J. Alexander García-Giraldo. "A comparative analysis of Cr(VI) reduction with Cu_2O , ZnO and Fe_2O_3 coatings grown by PEO", *Revista Facultad de Ingeniería Universidad de Antioquia*, no. 110, pp. 65-76, Jan-Mar 2024. [Online]. Available: <https://www.doi.org/10.17533/udea.redin.20230418>

ARTICLE INFO:

Received: February 04, 2022

Accepted: April 19, 2023

Available online: April 19, 2023

KEYWORDS:

Plasma electrolytic oxidation; Cu_2O ; ZnO; Fe_2O_3 ; photoreduction of Cr(VI)

Oxidación electrolítica con plasma; Cu_2O ; ZnO; Fe_2O_3 ; fotoreducción de Cr(VI)

ABSTRACT: Coatings on copper, zinc and stainless-steel substrates were fabricated using the plasma electrolytic oxidation (PEO) technique and their photocatalytic activity was evaluated in the reduction of Cr(VI), a highly toxic agent present in wastewater from industrial processes such as electroplating, manufacture of textile dyes, wood curing, and leather tanning. The concentration of hexavalent chromium in drinking water has been regulated to a maximum value established by national and international legislation of 0.05 ppm. The strategy of reduction to less toxic species such as Cr(III), followed by its precipitation in a basic medium, use several methods derived from chemistry, physics and biology for the treatment of water contaminated with this material. In the present work, some coatings of copper, zinc, and iron oxides were obtained over the corresponding metal sheets exposed to PEO, which were tested in a heterogeneous process of advanced oxidation with 1 ppm Cr(VI) solution under ultraviolet radiation. Thus, a reduction rate to Cr(III) close to 100% in 60 min was obtained.

RESUMEN: Se fabricaron recubrimientos sobre sustratos de cobre, zinc y acero inoxidable mediante la técnica de oxidación electrolítica con plasma (OEP) y se evaluó su actividad fotocatalítica en la reducción del Cr(VI), un agente altamente tóxico presente en las aguas residuales de procesos industriales como la galvanoplastia, la fabricación de tintes textiles, el curtido de la madera y el curtido del cuero. La concentración de cromo hexavalente en el agua potable se ha regulado hasta un valor máximo establecido por la legislación nacional e internacional de 0.05 ppm. La estrategia de reducción a especies menos tóxicas como el Cr(III), seguida de su precipitación en un medio básico fundamenta varios métodos de la química, la física y la biología para el tratamiento del agua contaminada con este material. En el presente trabajo, se obtuvieron recubrimientos de óxidos de cobre, zinc y hierro sobre las correspondientes láminas expuestas a OEP, que se ensayaron en un proceso heterogéneo de oxidación avanzada con una solución de 1 ppm de Cr(VI) bajo radiación ultravioleta. Así, se obtuvo una tasa de reducción a Cr(III) cercana al 100% en 60 min.

1. Introduction

Plasma Electrolytic Oxidation (PEO) has been reported in the fabrication of ceramic-type coatings on metals such as aluminum, titanium, magnesium, and alloys in order to increase their resistance to exposure and wear, improving

their tribological properties [1, 2]. In the particular case of titanium, this technique has been used for surface modification with the aim of obtaining the oxide of this metal, widely studied for its wide bandgap of forbidden energy, which makes it a good candidate for photocatalyst for pollutant charge reduction [3]. However, to guarantee the viability of this process at an industrial scale, it is important to explore the PEO with other metals, such as Zn, Cu, and stainless steel, costing \$3.78 [4], \$9.59 [5] and \$5 [6] per kilogram, respectively, which are cheaper than titanium (\$34.75) [7]. This study presents the results

* Corresponding author: Fernando Gordillo-Delgado

E-mail: fotocastica@uniquindio.edu.co

ISSN 0120-6230

e-ISSN 2422-2844



of Cr(VI) photoreduction using the coatings over these metallic substrates.

In some variations of conventional PEO, the substrate-electrode acts as the anode (anodic PEO), and the electrolyte container vessel or a platinum electrode is the cathode [8]; these methods include power supplies with variable or switchable output voltage at a given frequency and duty cycle [9]. This methodology allows control of the grain size of the oxide, directly formed on the substrate surface. Unlike conventional anodizing, in which low electrical voltages are used for exposure times longer than 20 min, the PEO involves the use of high magnitude voltages for less time.

The PEO consists of the surface modification of a metal that is immersed in an electrolyte solution contained in a metallic container. The concentration of the electrolyte determines the current intensity that flows through the substrate while it is subjected to an electrical voltage higher than the breakdown voltage of the material. When the breakdown voltage is exceeded, microdischarges are generated on the surface of the sample; thereby, the local pressure and temperature abruptly increase, producing microcavities. The current density can be controlled by considering the substrate shape and the applied electric potential [10].

Several processes use hexavalent chromium (Cr(VI)) to manufacture some products; in the automotive industry, one of them is electroplating or deposition of a metallic layer of chromium on objects to add reflective brightness and provide corrosion protection [11]; in the manufacture of paint and pigments, Cr(VI) is added to the product to improve its stability [12], and in the tannery, it is used to transform the collagen in the leather into a stable material to prevent its degradation and to increase its useful life [13, 14]. The Cr quantity that is not deposited, impregnated or absorbed in these techniques is returned to the environment through wastewater. This is harmful to health [15–17], so it is necessary to reduce Cr(VI) to Cr(III), which is less toxic and more environmentally friendly.

Although other reduction processes of hexavalent to trivalent chromium are currently used, such as bioremediation and chemical reactors [18–20], the fixation of materials for advanced oxidation presents advantages, such as the reuse of the catalyst, without complex recovery or addition of toxic agents.

The use of the cathodic configuration has been reported for PEO on certain metals and alloys; in this configuration, the substrate is placed as the cathode and the container vessel, or another electrode, as the anode [21]. Thus, several authors have modified stainless steel surfaces

decreasing the electric potential and low concentrations of the electrolyte [22]. In this work, the PEO anodic configuration was used with copper and zinc substrates, and the cathodic mode with the steel substrates. Based on the results, the existence of the corresponding oxides on each substrate and their efficiency in Cr(VI) photoreduction was probed; which do not have been reported before, in the best of our knowledge; most of the reports are related to oxide samples in powder for this application.

2. Materials and methods

Sheets of dimensions 20 mm x 20 mm x 1 mm of stainless steel (304), copper [Cu-DHP 1/2 hard CW024A] and zinc (shiny sheet EN 988) were previously polished with an abrasive paper and used as substrates. Before the PEO, these metal sheets were subjected to an ultrasonic bath for 20 min with distilled water and isopropanol. In all cases, the exposure time was 10 min, and a mixture of 0.2 g/L sodium metasilicate nonahydrate ($Na_2SiO_3 - 9H_2O$) and 0.05 g/L potassium hydroxide (KOH) was utilized as electrolyte.

The PEO of copper and zinc substrates was carried out by conventional mode with potential differences between the electrodes of 450, 550, 650 and 750 V, while the surface of stainless-steel substrates was modified with PEO cathodic configuration, applying 350, 450, and 550 V. In all cases, an INSTEK PSW 800-4.32 GW source was used by constant voltage mode. A schematic of the experimental setup for the PEO in anodic configuration is shown in the schema of Figure 1, in which the positive of the source was connected to the substrate-electrode and the negative to the metal vessel. In the cathodic arrangement, the polarity of the source leads was reversed.

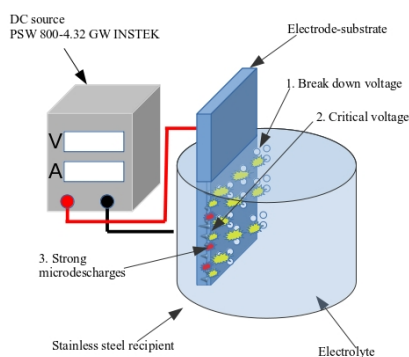


Figure 1 Experimental setup of the anodic PEO system

The X-ray diffractograms (XRD) of the samples were obtained with the grazing angle method, using an XBruker

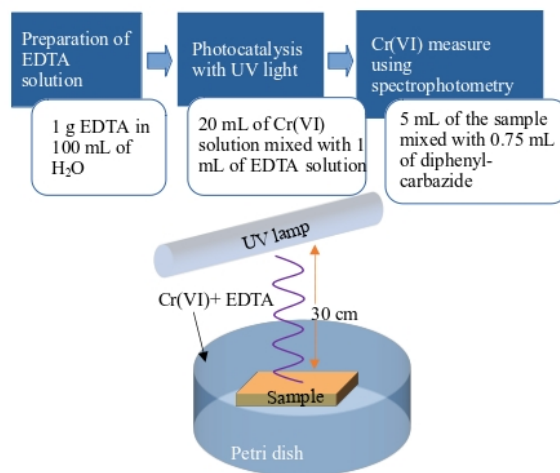


Figure 2 Schema of photocatalytic method (top) and experimental setup (bottom)

D8-Advance equipment, with a scan between 20° and 90°, at 5 s per degree, an operating voltage of 40 kV and current of 8 mA. The average crystalline size (*S*) of the coatings was estimated from XRD patterns, according to the Scherrer equation [Equation (1)] [23]:

$$S = \frac{K\lambda}{B \cos(\theta)} \quad (1)$$

Where β is the full width at half maximum (FWHM) in radian, corresponding to the most intense diffraction peak; $K = 0.9$ is the shape factor or Scherrer constant; λ is the X-ray wavelength of $CuK\alpha$ radiation (1.54056 Å) and θ is the Bragg's diffraction angle. The contributions of the crystallite size and lattice strain to diffraction peak broadening were calculated by the Williamson–Hall (WH) method, using Equation (2) [24]:

$$\beta \cos(\theta) = 0.9 \frac{K}{S} + 4\sigma \sin(\theta) \quad (2)$$

Where β is the measured FWHM of XRD, corresponding to different crystal planes, and σ is the effective strain.

The porous formation, cracks, and agglomerations during the growing of oxide layers could increase the surface-volume ratio, which has a direct influence on the photocatalytic activity. For this reason, in the present work, images of the coatings were taken with a JEOL JSM-5900LV Scanning Electron Microscope (SEM) to observe the sample surface morphology.

The physicochemical process of photoreduction involves the *in situ* generation of active radical species, especially hydroxyls, which lead to the destruction of pollutant targets. Therefore, a photocatalytic agent is used under the action of light in the presence of substances containing OH groups such as EDTA (ethylenediaminetetraacetic acid). A schema of the photocatalysis method is shown

in Figure 2. The photocatalytic activity was evaluated by irradiating the films, immersed in a solution of Cr(VI)-EDTA, with ultraviolet light of wavelength 255 nm from a 15 W bactericidal lamp. The complete reduction efficiency was obtained after 60 minutes. The test was performed in a climatic chamber, controlling the temperature to around 23 °C.

The standard method ASTM-3500 B-Cr [25] was applied to calculate the removal rate (*R*), using a spectrophotometer (EU-2800DS) to measure the absorbance of the sample solutions under the maximum absorbance wavelength (352 nm). Considering the direct relationship between concentration and absorbance, the *R* of Cr(VI) in the solution was calculated through Equation (3):

$$R(\%) = \frac{C_0 - C_f}{C_0} 100\% \quad (3)$$

Where C_0 and C_f are the initial and final Cr(VI) concentration, expressed in mg/L.

The kinetic model of the photocatalytic reaction, using the simplification to first-order that assumes isothermal conditions, can be expressed as follows [Equation (4)] [26]:

$$\ln \left(\frac{C_0}{C} \right) = k_r t \quad (4)$$

Where, C is the concentration at the time t and k_r is the rate constant of degradation.

In the experiments, three concentrations during the treatment of Cr(VI) aqueous solution were measured, so the analysis of experimental data was carried out with three points for the fit-linear process, using Equation (4). Although this number of points is low, the obtained values of the rate constant of degradation were only considered

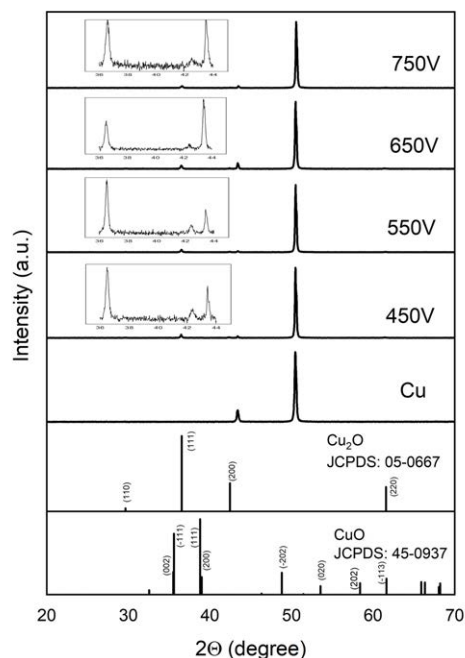


Figure 3 Diffractograms of copper substrates, modified by PEO with voltages between 450 and 750 V. In each case, the inserted plot corresponds to a magnification between 36 and 44°

Table 1 Grain sizes (S) of PEO coatings on copper substrates

Sample	Scherrer method S (nm)	WH method S (nm)	σ
450 V	47.78	128.97	0.0024
550 V	53.62	127.86	0.0018
650 V	48.23	83.8	0.0042
750 V	40.89	60.98	0.0052

as estimations for comparison purposes; although the behavior of these experimental points clearly showed a decrease of C/C_0 in the function of the exposition time, more data could be necessary to guarantee this information.

3. Results

3.1 Coatings of Cu_2O over Cu substrates

The diffractograms of the coatings of Cu substrate-electrode obtained with each PEO potential difference are shown in Figure 3. In the case of the pure copper substrate, two peaks were presented around 43.5° and 50.5°, which is similar to that reported by Theivasanthi and Alagar [27]. On the other hand, four

low-intensity peaks around 29.66°, 36.53°, 42.44° and 61.57° are observed, related to the (110), (111), (200) and (220) crystallographic directions of cuprous oxide (Cu_2O) [JCPDS: 05-0667], after surface modification by PEO [28, 29]. In any case, the formation of cupric oxide (CuO) was observed.

In Figure 4, the WH plots were made for all the observed diffraction peaks; the $\sin(\theta)$ values along the x-axis and $\beta \cos(\theta)$ values along the y-axis were drawn. The intercept with the y-axis of the best linear-fitting is related to the nanocrystalline size (S), and the slope gives the lattice strain multiplied by four (4σ). In Table 1, the corresponding values were registered. The S values obtained by Scherrer and WH methods are different due to the distribution of particle sizes in the sample [30]. It is possible to note that the size grain decreases while PEO voltage increases. On the other hand, the strain has a proportional behavior to this growth parameter, which suggests an increase in the dislocation density caused by this rising voltage.

The SEM micrograph of the 550 V-treated substrate, shown in Figure 5, indicates a surface modification with irregular topography of a flak-like shape.

The use of copper (I) and (II) oxides in the degradation of organic pollutants has been reported by other authors [31, 32]; these p-type semiconductors have a narrow bandgap of 1.2–1.8 eV and 2.0–2.2 eV, respectively, which allows their photoactivity with UV and visible light.

The photocatalytic activity of the Cu_2O coatings in the photoreduction of Cr(VI)-EDTA was evaluated through the data plotted in Figure 6. It can be seen a reduction rate close to 100% within 60 min with the samples, although with the coating grown at 450 V, the highest efficiency was achieved at 30 min of the process.

The k_r values were obtained from the slope of the linearly fitted plot in Figure 6 c) by using Equation (4), and the data were registered in Table 2. It is possible to see that the highest k_r value was obtained with the coating grown at 650 V PEO.

3.2 Coatings of ZnO over Zn substrates

The diffractograms in Figure 7 correspond to the PEO-modified zinc substrates. It can be observed the formation of zinc oxide related to the broad bands around 31.80, 34.47, 36.29, 47.60, 56.65, 62.94, 66.45, 68.03, and 69.16° [JCPDS: 036-1451], by which the intensity augmented as a function of increasing voltage. This is in agreement with those reported by other authors [33, 34]. In the experiments, once the plasma is obtained on

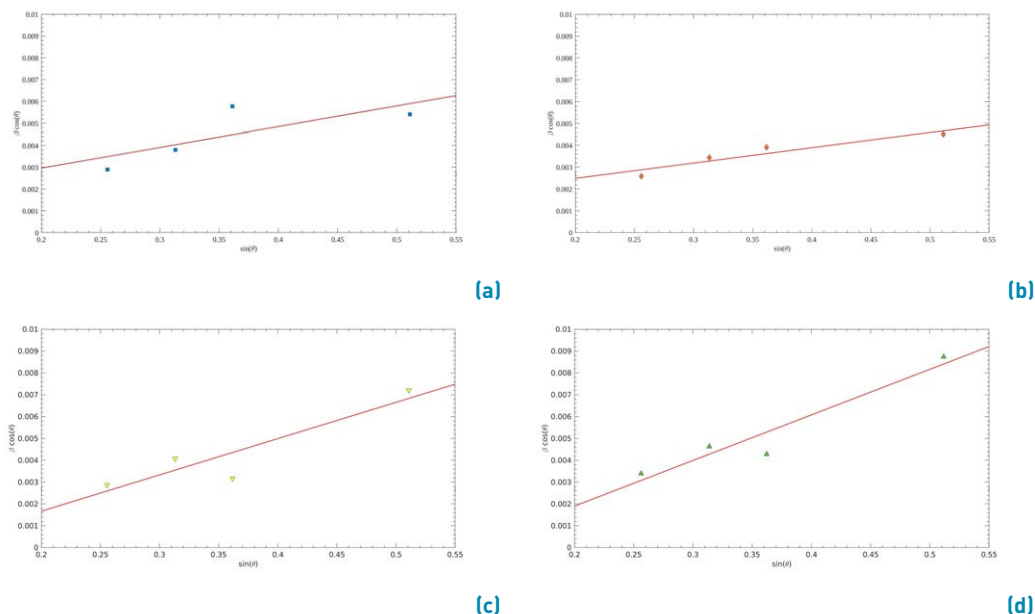


Figure 4 WH analysis corresponding to diffractograms in Figure 3 of Cu_2O coatings grown by PEO with voltages between a) 450, b) 550, c) 650, and d) 750 V. The continuous line represents the best linear-fitting for calculus of grain size of nanocrystals and strain effect

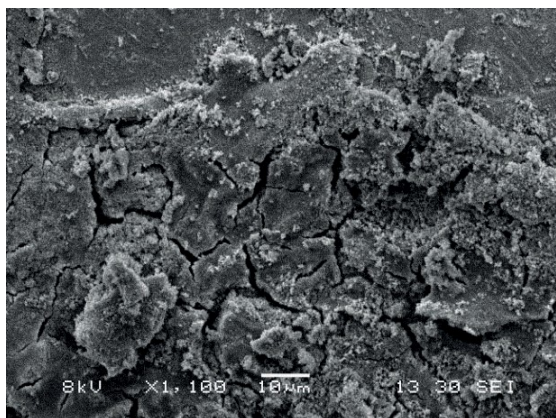


Figure 5 SEM micrograph of PEI-modified copper substrate at an electrical potential 550 V. The behavior was similar in the other samples

Table 2 The rate constant of degradation corresponding to analysis in Figure 6c) of degradation of Cr(VI)-EDTA with the Cu_2O coating samples. R^2 is the R-square statistic of the linear fitting

Sample	k_r (min^{-1})	R^2
450V	0.02	0.988
550V	0.02	0.999
650V	0.03	0.988
750V	0.02	0.995
Cu	0.001	0.999

the substrate surface, the current tends to be a constant value, but the electrolyte evaporates rapidly due to the high temperature reached, leading to the partial uncovering of the substrate-electrode. The band gap energy of this semiconductor material has been reported to be between 3.2 and 3.5 eV at room temperature [35, 36].

A SEM micrograph of the zinc substrate modified by PEI at 550 V is shown in Figure 9. In this case, the accumulation of irregular grains of different sizes and shapes distributed over the entire surface of the coating can be observed, which shows internal porosity and a sponge-like structure.

Table 3 Grain sizes (S) of the ZnO coatings

Sample	Scherrer method S (nm)	WH method S (nm)	σ
450V	27.16	20.12	0.0094
550V	10.75	7.92	-0.0053
650V	16.57	31.08	0.0044
750V	9	6.09	-0.0060

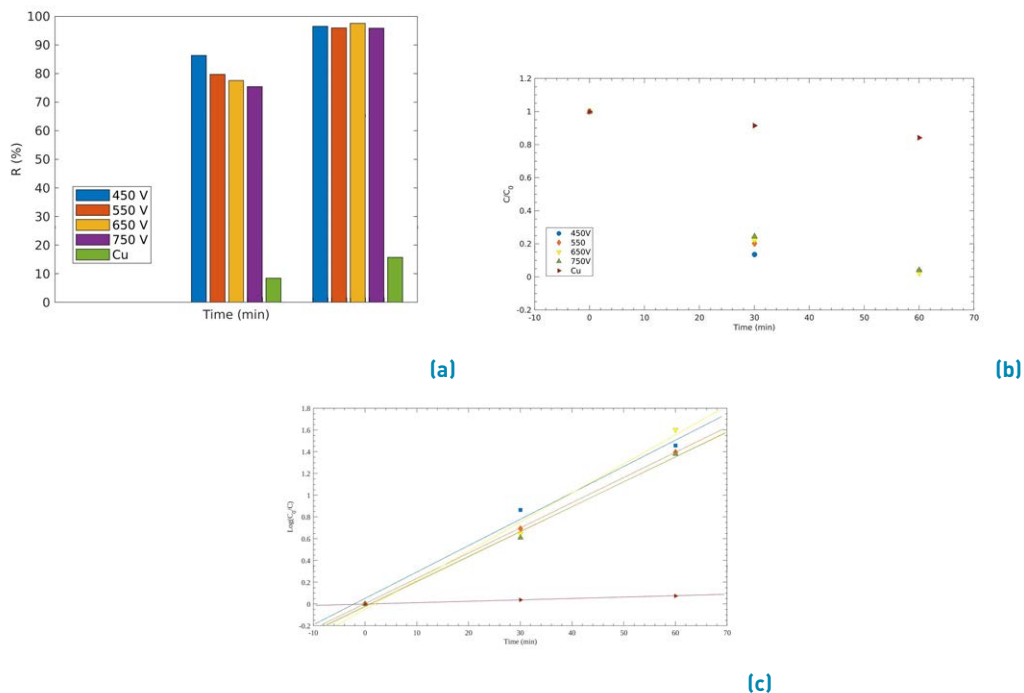


Figure 6 a) R (%), b) C/C_0 and c) $\log [C_0/C]$ of the photocatalytic process of the Cu_2O samples in the reduction of Cr(VI)-EDTA as a function of the exposition time. In this last plot, the solid line represents the best linear fitting

Table 4 The rate constant of degradation corresponding to the analysis in Figure 10c of degradation of Cr(VI)-EDTA with the ZnO coating samples

Sample	k_r (min^{-1})	R^2
450V	0.05	0.92
550V	0.05	0.93
650V	0.05	0.95
750V	0.05	0.96
Zn	0.01	0.99

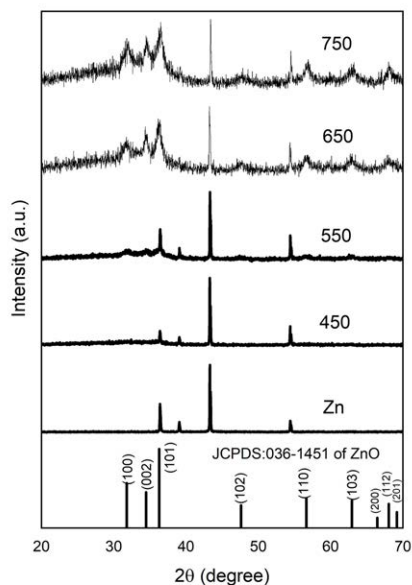


Figure 7 Diffractograms of PEO-modified zinc substrates at voltages between 450 and 650 V

concentration of 1 ppm. The reduction rates as a function of time are presented in Figure 10, showing a behavior similar to that described above for the Cu_2O coatings, reaching a reduction of around 100% within 60 min. The highest efficiency was achieved at 30 min with the samples obtained by PEO, using 650 and 750 V.

The k_r values, obtained from the slope of the linearly fitted plot in Figure 10c) by using Equation (4), were registered in Table 4. It is possible to see that k_r was the same for all ZnO coatings.

3.3 Coatings of Fe_2O_3 and Fe_3O_4 over stainless steel substrates

The photocatalytic performance of the ZnO coatings was tested in the reduction of Cr(VI)-EDTA with an initial

Substrate-electrodes of stainless steel 304 were treated by PEO, and its modified surface was analyzed to

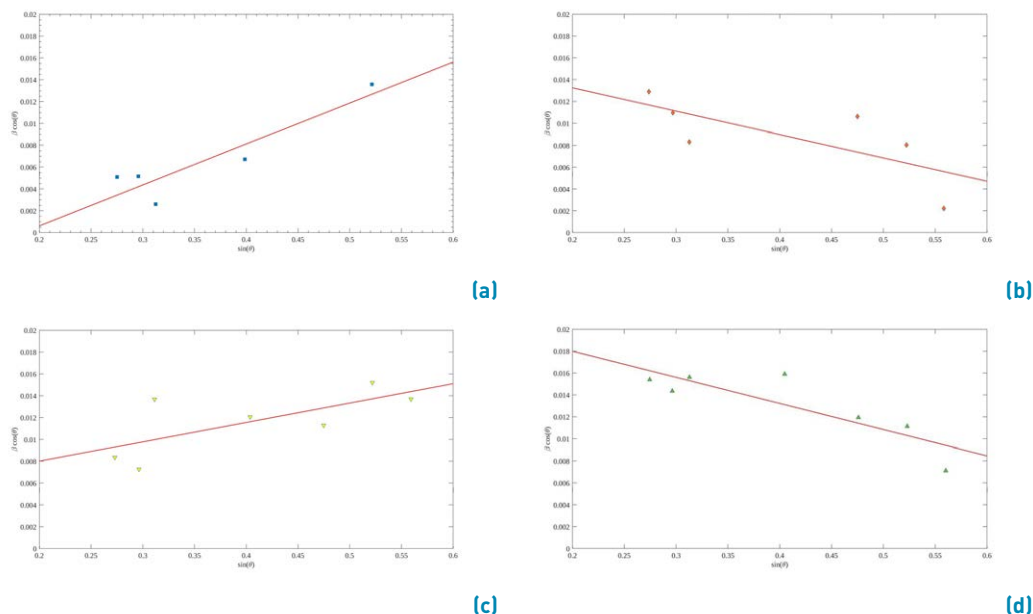


Figure 8 WH analysis corresponding to the diffractograms of PEO-modified zinc substrates using a) 450, b) 550 V, c) 650 V, and d) 750 V



Figure 9 SEM surface morphology of the ZnO sample, obtained by PEO with an electrical potential of 550 V. The behavior of the surface modification was similar using the other voltages

Table 5 Grain sizes (S) of Fe_2O_3 and Fe_3O_4 coatings on stainless steel 304 substrates

Sample	Scherrer (Fe_3O_4) S (nm)	Scherrer (Fe_2O_3) S (nm)	W-H S (nm)	σ
350V	17.28	21.45	10.49	-0.0034
450V	26.04	38.98	18.85	0.0070
550V	21.94	39.43	25.96	0.0054

search for the growth of iron oxides, known as Hematite (Fe_2O_3) and Magnetite (Fe_3O_4). These compounds have been reported in advanced oxidation process applications for textile industry wastewater treatment and as antibacterial for general purposes [37–39]. In Figure 11, the plotted diffractograms correspond to the coatings that were prepared by cathodic PEO, using 350, 450 and 550 V between the electrodes; the diffraction peaks were associated with the (2 0 2), (3 0 0) and (0 2 10) crystallographic planes of Fe_2O_3 (JCPDS: 330664); (6 2 2) of Fe_3O_4 (JCPDS 190629) and (2 0 0) of $\gamma - Fe$ (ICCD 98-004-1506). This intensity changed for the samples according to the surface modification of the steel sheet by cathodic PEO [40, 41].

In Figure 12, the WH plots were made for all the observed diffraction peaks corresponding to Fe_2O_3 . The intercept with the y-axis of the best linear-fitting is related to S and from the slope was estimated σ . In Table 5, the corresponding values were registered. The S values obtained by Scherrer and WH methods for both Fe_2O_3 and Fe_3O_4 are different, due to the distribution of particle sizes in the sample [26]. It is possible to note that the grain size increases while PEO voltage rises. On the other hand, the strain was negative for the lowest voltage and the strain minimum was obtained with the highest voltage.

From Figure 13, two SEM micrographs of the surface of the steel substrate modified by PEO at 550 V can be observed. The formation of crater-like pores and spheroidal nodules over the coating is observed, which increases the surface area, enhancing its photocatalytic activity. This morphology is different from that obtained by other authors, using cathodic PEO with a pulsed DC power supply; for instance, Jin *et al.* reported a surface in some hill-shaped embossment, employing voltages low 280 V [42], while Wu *et al.*, found a rough surface with some granular bulges under 400 V [43]. This behavior is as

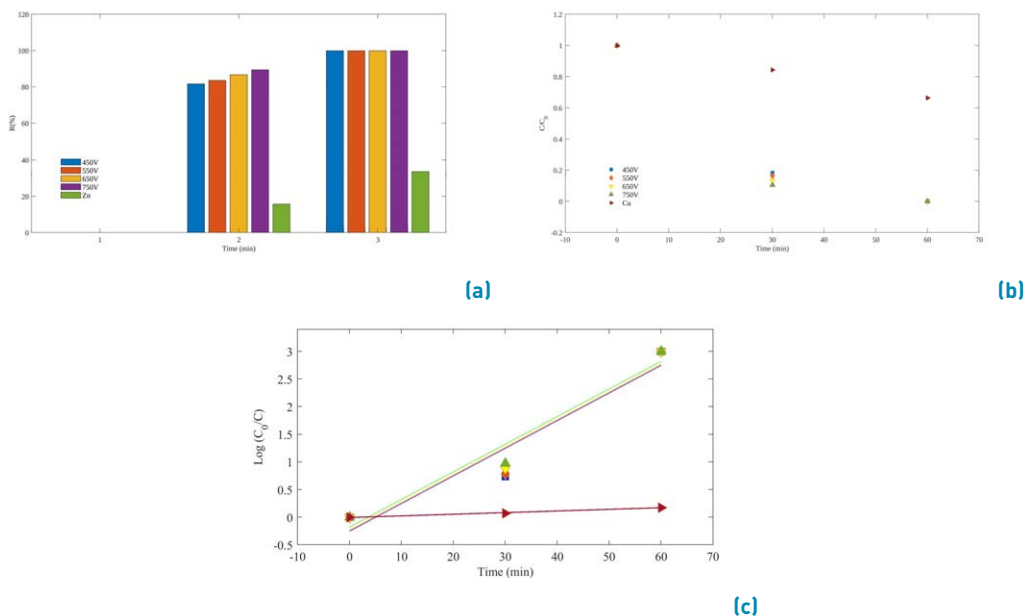


Figure 10 Photocatalytic efficiency of Cr(VI)-EDTA reduction with PEO-modified zinc sheets at electric potentials of 450, 550, 650, and 750 V

Table 6 The rate constant of degradation corresponding to analysis in Figure 14 c) of degradation of Cr(VI)-EDTA with Fe_2O_3 and Fe_3O_4 coating samples

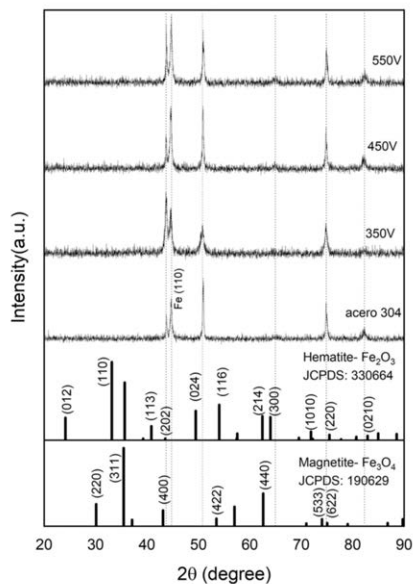


Figure 11 Diffractograms of PEO-modified 304 stainless steel substrates with inter-electrode voltages of 350, 450, and 550 V

Sample	k_r (min^{-1})	R^2
350V	0.02	0.92
450V	0.02	0.94
550V	0.03	0.88
steel	0	0.995

In Figure 14, the reduction behavior of Cr(VI)-EDTA using the PEO-modified stainless steel sheets is shown. A complete reduction was found within 60 min, using the samples obtained at 550 and 650 V. The k_r values obtained from the slope of the linearly fitted plot in Figure 14c) by using Equation (4) were registered in Table 6. It is possible to see that the highest k_r value was achieved with the coating grown at 550 V during the PEO.

The obtained coatings had a morphology that depended on the type of substrate. For the copper, the flak-like shape structures over the surface were grown, while for zinc substrate-electrodes, it can be seen agglomerations of the zinc oxide have a sponge-like appearance. In contrast, stainless steel crater-like microcavities, and spheroidal nodules were generated over its surface. This may be related to the fact that this material contains other elements such as chromium, manganese, and nickel, apart from iron and carbon; thus, other types of bonds can be produced on the surface of the substrate, and the topography of the substrate changes [45].

expected, because the effects of spark discharges can be mitigated by the application of pulsed current, providing control over the impact of plasma discharge on the surface [44].

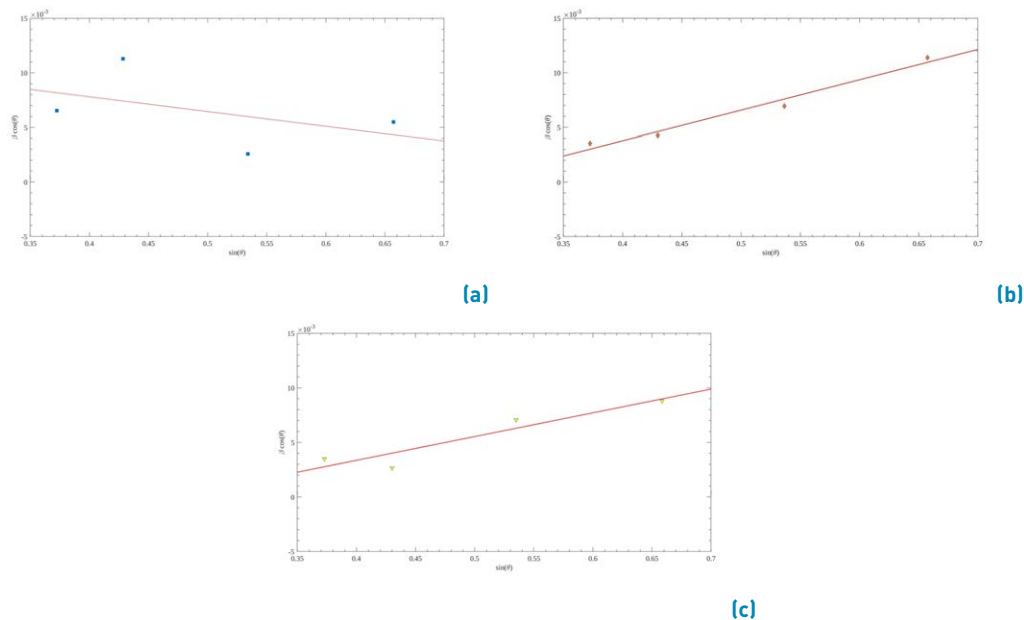
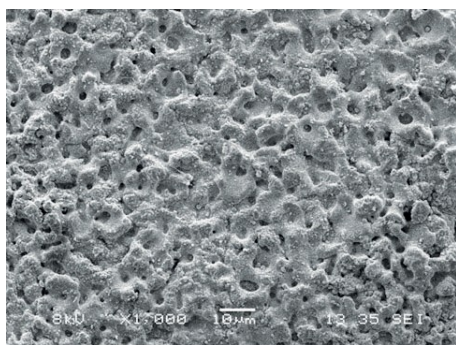
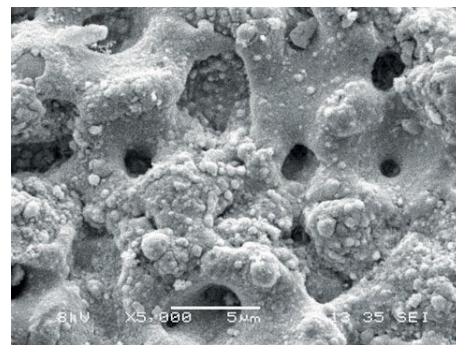


Figure 12 WH analysis corresponding to the diffractograms of PEO-modified stainless steel substrates using a) 350, b) 450 V, and c) 550 V



(a)



(b)

Figure 13 SEM micrographs of the surface of stainless-steel substrate modified by PEO with 550 V, using a magnification of a) X1000 and b) X5000

The high-energy processes, such as the PEO, promote the formation of new compounds that cannot be obtained by conventional chemical or physical methods [46]. Particularly for soft metals, the melting point plays an important role; this temperature for copper is 1357.77 K, while for zinc is 692.68 K, so the modification of surfaces by PEO with different characteristics in both such cases is expected.

According to the estimated values of k_r , the highest photocatalytic efficiency of Cr(VI) reduction was achieved using the ZnO coatings, possibly due to the wide bandgap of this semiconductor. However, the size grain did not have an influence in these results.

To compare the obtained results about reduction of Cr(VI) to Cr(III) with the reports of other authors, it was necessary to consider nanoparticle photocatalysts because corresponding studies with pure oxide coatings were not found. In this way, for example, with ZnO nanoparticles prepared by co-precipitation method with an average size of 20–50 nm, the photocatalytic ability of Cr(VI) reduction was 90% under UV-light irradiation for 17 h with and $k_r = 0.025 \text{ min}^{-1}$ [47], while in the present work, this value was doubled.

On the other hand, with Cu_2O , the corresponding reduction rate of Cr(VI) was $k_r = 0.00294 \text{ min}^{-1}$, under visible light irradiation, according to Xincheng-Dou *et al.* [48], which is a value 90% less than that reported in this work, but using UV-light radiation.

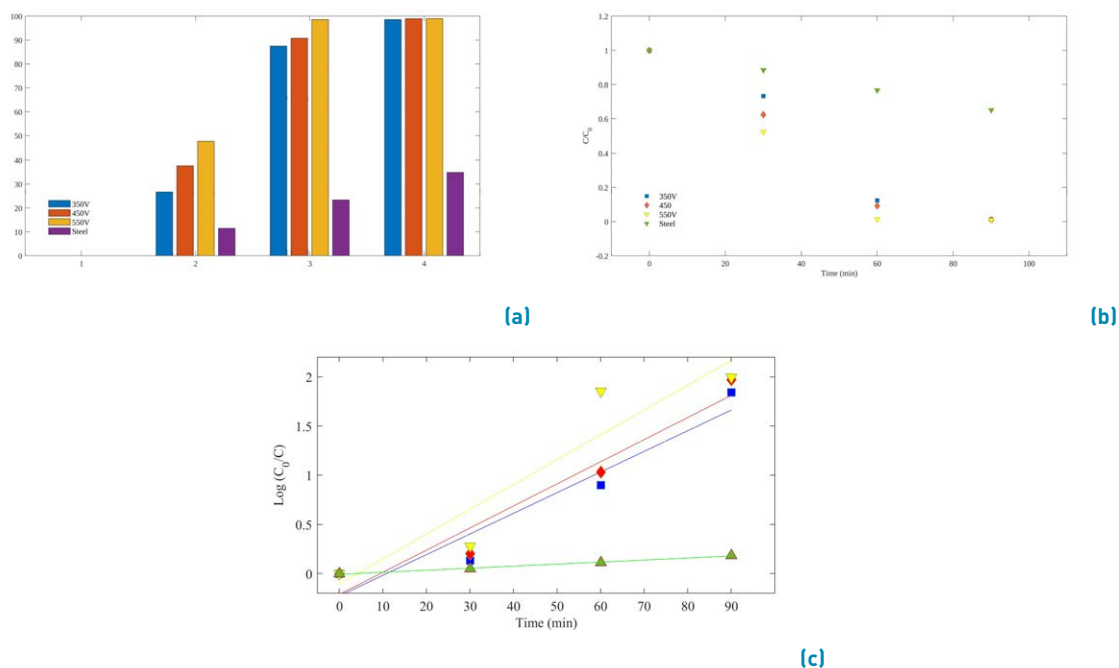


Figure 14 Cr(VI)-EDTA reduction rate with PEO-modified stainless steel sheets at voltages of 350, 450, and 550 V

Liu TY *et al.* reported that k_r ranged from 0.0072 min^{-1} to 0.0304 min^{-1} , using dosages between 0.5 and 3 g/L of Fe_2O_3 nanoparticles [49]; while pure Fe_3O_4 nanoparticles hardly reduced Cr(VI) within 90 min under visible light irradiation with a value of $k_r = 0.008 \text{ cm}^{-1}$, as reported by Ting-Ge *et al.* [50]. In contrast, in this work, with coatings containing both Fe_3O_4 and Fe_2O_3 , a $k_r = 0.03 \text{ min}^{-1}$ was found, a similar value to that maximum reported by Liu TY *et al.*

4. Conclusions

The PEO modification of the surfaces of the copper, zinc, and stainless-steel substrates was obtained by varying the voltage between the electrodes. The formation of layers of Cu_2O , ZnO and Fe_2O_3 and Fe_3O_4 , over each corresponding material, was verified by X-ray diffraction. As a growth parameter, this differential of potential affected the crystalline structure of the coatings since the intensity and width of the peaks changed in the related diffractograms. On the other hand, according to the micrographs of the surface of the samples, the morphology of the coating depends on the current demand and the characteristics of the power supply to support the output voltage.

The lattice strain factor had an important role in the formation of the nanocrystalline Cu_2O coatings; this was evidenced in the differences between estimated sizes with

Scherrer and WH methods. Using the sample grown to 650 V, the rate of degradation of Cr(VI) was slightly higher than those obtained with the others coatings on the Cu substrates. On the other hand, the strain factor had a low influence on the generation of ZnO, Fe_2O_3 , and Fe_3O_4 nanostructures, which can be inferred from the minor alteration of the grain size, calculated with both models, Scherrer and WH. While the rate of degradation with the coatings containing Fe_2O_3 and Fe_3O_4 was similar to that obtained with Cu_2O , the highest value of this parameter was achieved using the ZnO coatings.

Using ultraviolet radiation over the samples, the total photoreduction of Cr(VI)-EDTA was obtained within 60 minutes. For this reason, these coatings have the potential for use in the treatment of chromium-containing wastewater. In particular, PEO-treated stainless steel can be the best candidate, due to its high porosity corresponding to uniformly distributed microcavities.

5. Declaration of competing interest

We declare that we have no significant competing interests, including financial or non-financial, professional, or personal interests interfering with the full and objective presentation of the work described in this manuscript.

6. Acknowledgements

The authors thank the Universidad del Quindío for partial funding of this work through projects 982 and 1071 and the Instituto Interdisciplinario de las Ciencias for the XRD measurements. García-Giraldo expresses his gratitude to Minciencias and Universidad del Quindío for the Young Researcher grant.

7. Funding

This work was supported by Universidad del Quindío and Minciencias.

8. Author contributions

F. G. D conceived and designed the analysis. J. A. G. collected the data and contributed to the analysis tools. F. G. D and J.A.G wrote the paper.

9. Data availability statement

The authors confirm that the data supporting the findings of this study are available within the article [and/or] its supplementary materials.

References

- [1] S. Aliasghari, P. Skeldon, and G.E. Thompson, "Plasma electrolytic oxidation of titanium in a phosphate/ silicate electrolyte and tribological performance of the coatings," *Applied Surface Science*, vol. 316, Oct. 15, 2014. [Online]. Available: <https://doi.org/10.1016/j.apsusc.2014.08.037>
- [2] K. C. Tekin, U. Malayoglu, and S. Shrestha, "Tribological properties of plasma electrolytic oxide coatings on magnesium alloys," *Tribology - Materials, Surfaces and Interfaces*, vol. 6, no. 2, 2012. [Online]. Available: <https://doi.org/10.1179/1751584X12Y.0000000006>.
- [3] F. Gordillo-Delgado, S. Moya-Betancur, A. Parra-López, J. García-Giraldo, and D. Torres-cerón, "S-incorporated tio2 coatings grown by plasma electrolytic oxidation for reduction of cr(vi)-edta with sunlight," *Environmental Science and Pollution Research*, vol. 26, Feb. 20, 2019. [Online]. Available: <https://doi.org/10.1007/s11356-018-2695-6>
- [4] (n.d.) Zinc price. Markets Insider. [Online]. Available: <https://markets.businessinsider.com/commodities/zinc-price>
- [5] (n.d.) Cooper price. Markets Insider. [Online]. Available: <https://markets.businessinsider.com/commodities/copper-price>
- [6] (n.d.) 304/304l stainless steel plates. Savoy Piping Inc. [Online]. Available: <https://www.savoypipinginc.com/stainless-steel-plates-sheet-type/304-304l-stainless-steel-plates-stockholder-supplier-dual-grade.html>
- [7] (n.d.) Tin price. Markets Insider. [Online]. Available: <https://markets.businessinsider.com/commodities/tin-price>
- [8] S. M. Kumar, J. Youngjoo, K. Jongmin, K. Hyungtae, and J. J. Pil, "Plasma electrolytic oxidation in surface modification of metals for electronics," *Journal of Welding and Joining*, vol. 32, no. 3, Jun. 30, 2014. [Online]. Available: <https://doi.org/10.5781/JWJ.2014.32.3.27>
- [9] V. Dehnavia, B. LiLuan, D. W. Shoemsmith, X. Y. Liu, and S. Rohani, "Effect of duty cycle and applied current frequency on plasma electrolytic oxidation (peo) coating growth behavior," *Surface and Coatings Technology*, vol. 226, Jul. 15, 2013. [Online]. Available: <https://doi.org/10.1016/j.surfcoat.2013.03.041>
- [10] M. Kaseem, S. Fatimah, N. Nashrah, and Y. GunKob, "Recent progress in surface modification of metals coated by plasma electrolytic oxidation: Principle, structure, and performance," *Progress in materials science*, vol. 117, Apr. 2021. [Online]. Available: <https://doi.org/10.1016/j.pmatsci.2020.100735>
- [11] C. Oduoza, E. Khan, and T. Sihra, "Chromium electroplating of aluminium alloys using electroless nickel as underlayer," *Journal of Materials Science and Chemical Engineering*, vol. 7, no. 2, Jul. 2014. [Online]. Available: <https://doi.org/10.4236/msce.2014.27007>
- [12] F. C. Izzo, K. J. V. den Berg, H. V. Keulen, B. Ferriani, and E. Zendri, "Modern oil paints- formulations, organic additives and degradation: some case studies," in *Issues in contemporary oil paint*, C. Springer, Ed. Suiza, CH: Springer, 2014, pp. 75-104.
- [13] A. L. Tasca and M. Puccini, "Leather tanning: Life cycle assessment of retanning, fatliquoring and dyeing," *Journal of Cleaner Production*, vol. 226, Jul.20, 2019. [Online]. Available: <https://doi.org/10.1016/j.jclepro.2019.03.335>
- [14] D. Hansen, P. Aquim, and M. Gutterres, "Environmental assessment of water, chemicals and effluents in leather post-tanning process: A review," *Environmental Impact Assessment Review*, vol. 89, Jul. 2021. [Online]. Available: <https://doi.org/10.1016/j.eiar.2021.106597>
- [15] C. C. Alvarez, M. E. B. Gómez, and A. H. Zavala, "Hexavalent chromium: Regulation and health effects," *Journal of Trace Elements in Medicine and Biology*, vol. 65, no. 126729, May. 2021. [Online]. Available: <https://doi.org/10.1016/j.jtemb.2021.126729>
- [16] T. L. DesMarias and M. Costa, "Mechanisms of chromium-induced toxicity," *Current Opinion in Toxicology*, vol. 14, Apr. 2019. [Online]. Available: <https://doi.org/10.1016/j.cotox.2019.05.003>
- [17] R. Saha, R. Nandi, and B. Saha, "Sources and toxicity of hexavalent chromium," *Journal of Coordination Chemistry*, vol. 64, no. 10, May. 2011. [Online]. Available: <https://doi.org/10.1080/00958972.2011.583646>
- [18] J. Wang, S. Zhao, Z. Ling, T. Zhou, P. Liu, and *et al.*, "Enhanced removal of trivalent chromium from leather wastewater using engineered bacteria immobilized on magnetic pellets," *Science of The Total Environment*, vol. 775, no. 145647, Jun. 25 2021. [Online]. Available: <https://doi.org/10.1016/j.scitotenv.2021.145647>
- [19] S. Mishra, S. Chen, G. D. Saratale, R. G. Saratale, L. F. R. Ferreira, and *textitet al.*, "Reduction of hexavalent chromium by microbacterium paraoxydans isolated from tannery wastewater and characterization of its reduced products," *Journal of Water Process Engineering*, vol. 39, no. 101748, Feb. 2021. [Online]. Available: <https://doi.org/10.1016/j.jwpe.2020.101748>
- [20] S. S. Kerur, S. Bandekar, M. S. Hanagadakar, S. S. Nandi, G. M. Ratnamala, and *textitet al.*, "Removal of hexavalent chromium-industry treated water and wastewater: A review," *Materials Today: Proceedings*, vol. 42, no. 2, Mar. 2021. [Online]. Available: <https://doi.org/10.1016/j.matpr.2020.12.492>
- [21] M. Aliofkhazraei, A. S. Rouhaghdam, and P. Gupta, "Nano-fabrication by cathodic plasma electrolysis," *Critical Reviews in Solid State and Materials Sciences*, vol. 36, no. 3, Sep. 2, 2011. [Online]. Available: <https://doi.org/10.1080/10408436.2011.593269>
- [22] W. Gui, J. Lin, G. Hao, Y. Qu, Y. Liang, and *et al.*, "Electrolytic plasma processing-an innovative treatment for surface modification of 304 stainless steel," *Scientific Reports*, vol. 7, no. 308, Mar. 22, 2017. [Online]. Available: <https://doi.org/10.1038/s41598-017-00204-w>
- [23] H. G. Jiang, M. Rühle, and E. J. Lavernia, "On the applicability of the x-ray diffraction line profile analysis in extracting grain size and microstrain in nanocrystalline materials," *Journal of Materials Research*, vol. 14, no. 22, pp. 549-559, 1999.
- [24] M. Birkholz, *Thin film analysis by X-ray scattering*. John Wiley & Sons, 2006.
- [25] A. Apha, *Standard methods for the examination of water and wastewater*, 23rd ed. Washington, DC: American Public Health Association and American Water Works Association and Water

- Environment Federation, 2007.
- [26] M. Pirhashemi and A. H. Yangjeh, "Simple and large scale one-pot method for preparation of agbr-zno nanocomposites as highly efficient visible light photocatalyst," *Applied Surface Science*, vol. 283, pp. 1080–1088, Oct. 2013.
- [27] T. Theivasanthi and M. Alagar, "X-ray diffraction studies of copper nanopowder," *Archives of Physics Research*, vol. 1, no. 2, pp. 112–117, Mar. 2010.
- [28] S. F. Shaffiey, M. Shapoori, A. Bozorgnia, and M. H. Ahmadi, "Synthesis and evaluation of bactericidal properties of cuo nanoparticles against aeromonas hydrophila," *Nanomedicine Journal*, vol. 1, no. 3, pp. 198–204, Apr. 2014.
- [29] N. G. Elfadill, M. R. Hashim, K. M. Chahrour, M. A. Qaeed, and W. Chunsheng, "The influence of oxygen pressure on the growth of cuo nanostructures prepared by rf reactive magnetron sputtering," *Journal of Materials Science: Materials in Electronics*, vol. 25, no. 1, Jan. 2014. [Online]. Available: <https://doi.org/10.1007/s10854-013-1581-8>
- [30] A. K. Zak, R. Razali, W. A. Majid, and M. Darroudi, "Synthesis and characterization of a narrow size distribution of zinc oxide nanoparticles," *International Journal of Nanomedicine*, vol. 6, pp. 1399–1403, Jul. 2011.
- [31] D. D. Arhin, E. E. Mbu, S. K. Ntwampe, E. N. Malenga, E. F. Kankeu, and *et al.*, "Synthesis of nanostructured cupric oxide for visible light assisted degradation of organic wastewater pollutants," *Cogent Engineering*, vol. 8, no. 1, 2021. [Online]. Available: <https://doi.org/10.1080/23311916.2021.1920563>
- [32] A. Khataeeand, D. Kalderis, P. YekanMottlagh, V. Binas, and S. Stefaet *al.*, "Synthesis of copper (i, ii) oxides/hydrochar nanocomposites for the efficient sonocatalytic degradation of organic contaminants," *Journal of Industrial and Engineering Chemistry*, vol. 95, Mar. 25, 2021. [Online]. Available: <https://doi.org/10.1016/j.jiec.2020.12.006>
- [33] S. Talam, S. R. Karumuri, and N. Gunnam, "Synthesis, characterization and spectroscopic properties of zno nanoparticles," *ISRN Nanotechnology*, 2012. [Online]. Available: <https://doi.org/10.5402/2012/372505>
- [34] S. Stojadinović, N. Tadić, and R. Vasilčić, "Formation and characterization of zno films on zinc substrate by plasma electrolytic oxidation," *Surface and Coatings Technology*, vol. 307, Dec. 15, 2016. [Online]. Available: <https://doi.org/10.1016/j.surfcoat.2016.09.080>
- [35] V. Srikant and D. R. Clarke, "On the optical band gap of zinc oxide," *Journal of Applied Physics*, vol. 83, no. 10, 1998. [Online]. Available: <https://doi.org/10.1063/1.367375>
- [36] A. Janotti and C. G. V. de Walle, "Fundamentals of zinc oxide as a semiconductor," *Reports on Progress in Physics*, vol. 72, no. 12, Oct. 22, 2009. [Online]. Available: <https://doi.org/10.1088/0034-4885/72/12/126501>
- [37] S. P. Schwaminger, R. Surya, S. Filser, A. Wimmer, F. Weigl, and *et al.*, "Formation of iron oxide nanoparticles for the photooxidation of water: Alteration of finite size effects from ferrihydrite to hematite," *Scientific Reports*, vol. 7, no. 1, Oct. 13, 2017. [Online]. Available: <https://doi.org/10.1038/s41598-017-12791-9>
- [38] S. Bakardjieva, V. Stengl, J. Subrt, V. Houskova, and P. Kalenda, "Photocatalytic efficiency of iron oxides: degradation of 4-chlorophenol," *Journal of Physics and Chemistry of Solids*, vol. 68, no. 5-6, 2007. [Online]. Available: <https://doi.org/10.1016/j.jpcs.2006.12.004>
- [39] M. M. Rafi, K. S. Zameer, K. PremNazeer, and D. S. Kumar, "Antibacterial activity of iron oxide nanoparticles on polysaccharide templates: synthesis, characterization and magnetic studies," *Malaysian Polymer Journal*, vol. 10, no. 1, pp. 16–22, 2015.
- [40] A. Hosseinian, H. Rezaei, and A. R. Mahjoub, "Preparation of nanosized iron oxide and their photocatalytic properties for congo red," *World Academy of Science, Engineering and Technology*, vol. 52, no. 4, pp. 736–739, 2011.
- [41] K. A. Habib, M. S. Damra, J. J. Saura, I. Cervera, and J. Belles, "Breakdown and evolution of the protective oxide scales of aisi 304 and aisi 316 stainless steels under high-temperature oxidation," *International Journal of Corrosion*, vol. 2011, 2011. [Online]. Available: <https://doi.org/10.1155/2011/824676>
- [42] X. Jin, L. Che, J. Yu, R. Liu, W. Xue, and *et al.*, "Temperature measurement and oes analysis during cpeo on stainless steel," *Surface and Coatings Technology*, vol. 363, Apr. 15, 2019. [Online]. Available: <https://doi.org/10.1016/j.surfcoat.2019.02.013>
- [43] J. Wu, L. Dong, J. Deng, D. Hou, G. Li, and *et al.*, "Direct growth of oxide layer on carbon steel by cathodic plasma electrolysis," *Surface and Coatings Technology*, vol. 338, Mar. 25, 2018. [Online]. Available: <https://doi.org/10.1016/j.surfcoat.2018.01.080>
- [44] E. V. Partenov, A. Yerokhin, R. R. Nevyantseva, M. V. Gorbalkov, C. J. Liang, and *et al.*, "Towards smart electrolytic plasma technologies: An overview of methodological approaches to process modelling," *Surface and Coatings Technology*, vol. 269, May. 15, 2015. [Online]. Available: <https://doi.org/10.1016/j.surfcoat.2015.02.019>
- [45] J. L. Marulanda, S. I. Castañeda, and F. J. Perez, "Study microstructure and composition of oxidation in steam at 700 and 750°C of austenitic steels aisi 304, 316 and 317," *Revista Facultad de Ingeniería Universidad de Antioquia*, no. 67, pp. 98–111, 2013.
- [46] A. Top and H. Çetinkaya, "Zinc oxide and zinc hydroxide formation via aqueous precipitation: Effect of the preparation route and lysozyme addition," *Materials Chemistry and Physics*, vol. 167, Nov. 1, 2015. [Online]. Available: <https://doi.org/10.1016/j.matchemphys.2015.10.013>
- [47] Q. Q. Xu, S. W. Qiu, X. Y. Xing, Z. H. Wang, Y. T. Li, and *et al.*, "Tuning the morphology of zno nanoparticles by zn-clusters and application on the photoreduction of cr(vi)," *Solid State Sciences*, vol. 58, Aug. 2016. [Online]. Available: <https://doi.org/10.1016/j.solidstatedsciences.2016.05.010>
- [48] X. Dou, C. Zhang, and H. Shi, "The simultaneous promotion of cr (vi) photoreduction and tetracycline removal over 3d/2d cu2o/biobr s-scheme nanostructures," *Separation and Purification Technology*, vol. 282, Feb. 1, 2022. [Online]. Available: <https://doi.org/10.1016/j.seppur.2021.120023>
- [49] T. Y. Liu, L. Zhao, X. Tan, S. J. Liu, J. J. Li, and *et al.*, "Effects of physicochemical factors on cr(vi) removal from leachate by zero-valent iron and alpha-fe(2)o(3) nanoparticles," *Water Sci Technol*, vol. 61, no. 11, Jun. 10, 2010. [Online]. Available: <https://doi.org/10.2166/wst.2010.167>
- [50] T. Ge, Z. Jiang, L. Shen, J. Li, Z. Lu, and *et al.*, "Synthesis and application of fe3o4/fewo4 composite as an efficient and magnetically recoverable visible light-driven photocatalyst for the reduction of cr(vi)," *Separation and Purification Technology*, vol. 263, May. 15, 2021. [Online]. Available: <https://doi.org/10.1016/j.seppur.2021.118401>